Large Eddy Simulation of Backward Facing Step Flow

Balram Panjwani[‡]
e–mail: balram.panjwani@ntnu.no

Ivar S. Ertesvåg[‡], **Andrea Gruber**[†] **and Kjell Erik Rian**[†‡]
[‡] Department of Energy and Process Engineering,
Norwegian University of Science and Technology,Trondheim
[†]SINTEF Energy Research, Trondheim
[†‡]Computational Industry Technologies (ComputIT), N-7462 Trondheim, Norway

Summary The paper describes the implementation and applicability of the Large eddy simulation (LES) technique for simulating turbulent flows. The LES approach is implemented in the in-house RANS research code Spider-3D. The Spider-LES code is validated by studying the unsteady flow over a backward-facing step (BFS). The LES simulation over the BFS is carried out at a Reynolds number of 5100 based on the inlet free-stream velocity. Finite-volume discretization schemes for the non-linear convective terms and sub-grid stress (SGS) models used for LES approach are discussed in the present study. To investigate mesh dependency, two types of grid resolution are studied. The results computed from Spider-LES are validated against DNS reference data by Le et al. The mean longitudinal, vertical velocity profile and the turbulence intensities compare satisfactory with the DNS data at the normalized coordinates $X^* = (x - X_r)/X_r$. The reattachment length X_r in the longitudinal direction, varies from $7.2h$ to $7.4h$ with different SGS models used as compared to the DNS value of $6.28h$.

Introduction

Modeling of fluid flow by numerical simulations includes Reynolds Averaged Navier Stokes (RANS), Large Eddy Simulation (LES) and Direct Numerical Simulation (DNS). In RANS, statistical averaged flow quantities are computed and all turbulence effects are modeled. The method gives good predictions and has been successful in a wide range of industrial applications. The required turbulence modeling and statistical average will, nevertheless, always be an inherent weakness of RANS. On the other hand, DNS can be used to resolve turbulent flow without any turbulence modeling. Then, all length and time scales of the turbulent flows are resolved, from the largest scales governed by the geometry and boundary conditions and down to the Kolmogorov scales. A very fine resolution in space and time together with high order differencing schemes will then be required. This makes DNS computationally expensive, especially at high Reynolds numbers. When applied to combustion problems, e.g. [13], the computational requirements to a full DNS is vastly increased, typically by 10-20 orders of magnitude [8] compared to modeling of non-reacting flows. LES is a promising tool for understanding the physics of unsteady turbulent flow at reduced costs. In LES, the large geometrically dependent energy-carrying eddies are resolved on grid scales(GS), whereas effects of the smaller, more universal scales are modeled using a sub-grid scale (SGS) model. A high fidelity LES should resolve length scales from the largest to the inertial scale on the grid scales. Wide range of subgrid models have been studied and successfully applied to LES [35, 23, 2, 9].

The LES approach was first used by Smagorinsky [38] and Lilly [24]. Since then the technique has been used in engineering applications such as channel flows, combustion, automotive, nuclear power engineering, etc. The literature shows comprehensive reviews of the theories, implementations, applications and limitations of the LES approach, e.g. [35, 23, 2, 9]. The accuracy of the fluid flow modeling with LES depends on the discretization scheme, the grid resolution and the subgrid-scale (SGS) model. In LES, numerical diffusion caused by the truncation error of a

low-order finite-volume discretization scheme (FVDS) can be of the same order of magnitude as the turbulence viscosity [22, 18]. Ideally, in LES, all scales down up to the inertial subrange should be resolved. The turbulence near a solid wall is, however, inhomogeneous, not in equilibrium and shear plays a significant role. In short, there is no inertial subrange. Therefore large number of grid points are required to resolve the turbulence near to the wall, which makes LES computationally expensive. Hence, the SGS model plays a significant role in regions close to the wall [33]. Influence of numerical schemes, grid resolution and the subgrid-stress models on the LES of turbulent flow for engineering and academic problems have been studied by many authors, e.g. [32, 19].

The present study focusing on fluid flow modeling is part of a larger effort to develop LES for industrial combustion flow applications. Chemical reactions mainly occur in the small scale structures of the turbulence. Hence, the combustion modeling in LES is closely related to that of RANS. Moreover, the accuracy of fluid flow modeling is decisive for the combustion modeling. The code used is an in-house code known as Spider, which is developed in curvilinear, non-orthogonal coordinates. The RANS version has been successfully used for a wide range of reacting and non-reacting academic and industrial flow problems, e.g. [26, 28, 27, 11, 12]. In this study, LES has been implemented in the code and the future aim is to use Spider-LES for reacting flow with complex geometries. For the time being, most LES applications are limited to simple geometry. A generalized curvilinear coordinate based numerical algorithm applicable for practicable geometries will be required. Therefore, in the present paper, the LES approach is described in the generalized curvilinear coordinates concerning the discretization schemes for non-linear convective terms and SGS stress modeling. The model is validated by solving the unsteady turbulent flows, i.e., flow over a backward facing step (BFS). Although the BFS flow is geometrically simple and does not require any coordinate transformation, but it involves very complex phenomena. In Spider-LES, for an orthogonal grid (BFS), contribution from the non-orthogonal terms will not be computed.

The main objective of the study was to understand the influence of the SGS modelling, discretization schemes and grid refinement in the BFS flow. At the corner of the step, the separated upstream boundary layer forms a free-shear layer. The free shear-layer attaches downstream at the reattachment point X_r and the reattachment point X_r oscillate in longitudinal direction. The fluid, upstream to the reattachment point is subjected to an adverse pressure gradient and forms a separation bubble. The turbulence length scales in the recirculation region are limited by the step height [43, 7]. Non-reacting flows over backward facing steps have been studied extensively both experimentally and numerically, and it is one of the benchmark test cases in turbulence modeling. Eaton and Johnston [7] have reviewed the BFS data base to establish the influences of system parameters (inflow boundary layer thickness, freestream turbulence, streamwise pressure gradient, etc.) on the shear-layer reattachment. Westphal and Johnston [43] studied the effects of initial conditions on the reattachment of the shear-layer experimentally. Jovic and Driver [17] have conducted experiments on the BFS at a Reynold number of 5100 and at the same Reynolds number Le et al. [21] carried out a direct numerical simulation with a grid resolution of ($768 \times 192 \times 64$). The DNS showed good agreement with experiments. Further Aider and Danet [1] have carried out a LES simulation of BFS to establish the influences of inflow boundary condition on the reattachment length. Meri and Wengle [29] and Simons et al. [37] have studied the influences of numerical scheme on the reattachment length. They

concluded that the LES solutions for turbulent flow over a backward-facing step was a complex interplay between the grid resolution, accuracy of the numerical scheme and SGS modeling. The present paper will shed more light on the influences of numerical scheme, subgrid model and grid resolution for a flow over the BFS.

Governing equations

Three dimensional time dependent Navier-Stokes equations in generalized curvilinear coordinate in strong conservation law form [42] are used in present LES simulation [16, 35, 18].
Continuity equation for flows with constant density

$$\frac{\partial \rho J U^k}{\partial \xi^k} = 0 \tag{1}$$

The momentum equation can be expressed as

$$\frac{\partial \rho J u_i}{\partial t} + \frac{\partial \rho J U^k u_i}{\partial \xi^k} = -\frac{\partial J \xi_i^k p}{\partial \xi^k} + \frac{\partial}{\partial \xi^k}\left(\mu J \xi_j^k \left(\xi_j^l \frac{\partial u_i}{\partial \xi^l} + \xi_i^l \frac{\partial u_j}{\partial \xi^l}\right)\right) \tag{2}$$

Where, summation rule applies to all indices except indices i, u_i denotes the Cartesian component of velocity field, ρ is the density, p is the static pressure, μ is the dynamic viscosity, ξ^k is the coordinate direction in the transformed space, $\xi_j^k = \partial \xi^k / \partial x_j$, J is the Jacobian of coordinate transformation, and $U^k = \xi_j^k u_j$ is the contravariant velocity component. This form of the equation is given as the code was developed [26, 28, 27] in general curvilinear coordinates with Cartesian components of the velocities and stresses.
In the LES, a spatial low-pass filter $G\left(\xi^j - \xi^{j'}\right)$ is introduced to obtain the filtered field $\overline{\phi}\left(\xi^j, t\right)$ from the full unresolved field $\phi\left(\xi^j, t\right)$. Where $\xi^{j'}$ denotes local coordinate direction in the transformed space and at center of the cell $\xi^{j'} = 0$. The filtering operation is expressed as [16]

$$\overline{\phi}\left(\xi^j, t\right) = \int_{-\infty}^{\infty}\!\!\!\int\!\!\!\int \phi\left(\xi^{j'}, t\right) G\left(\xi^j - \xi^{j'}\right) d\xi^{1'} d\xi^{2'} d\xi^{3'} \tag{3}$$

The box Filter

$$G\left(\xi^j - \xi^{j'}\right) = \begin{cases} \frac{1}{\Delta^j} & \text{if } |\xi^j - \xi^{j'}| \leq \frac{\Delta^j}{2} \\ 0 & \text{otherwise} \end{cases} \tag{4}$$

Where Δ^j is the local filter width in the curvilinear direction ξ^k. Implicit filtering is used here for obtaining the filtered N-S equations. The implicit filtering process refers to volume averaging over local cell, which is default with finite volume schemes. The implicit filter is the box filter with filter width Δ^j equal to the the local mesh size $\Delta\xi^j$.

$$\overline{\phi}\left(\xi^j, t\right) = \prod_{k=1}^{3} \frac{1}{\Delta \xi^k} \int_{\xi^3 - \Delta\xi^3/2}^{\xi^3 + \Delta\xi^3/2} \int_{\xi^2 - \Delta\xi^2/2}^{\xi^2 + \Delta\xi^2/2} \int_{\xi^1 - \Delta\xi^1/2}^{\xi^1 + \Delta\xi^1/2} \phi\left(\xi^{j'}, t\right) d\xi^{1'} d\xi^{2'} d\xi^{3'} \tag{5}$$

The filtered continuity equation for flows with constant density:

$$\frac{\partial J \overline{U^k}}{\partial \xi^k} = 0 \tag{6}$$

The filtered momentum equation

$$\frac{\partial J\overline{\rho}\,\overline{u_i}}{\partial t}+\frac{\partial \overline{\rho} J\overline{U^k}\overline{u_i}}{\partial \xi^k}=-\frac{\partial J\xi_i^k\overline{p}}{\partial \xi^k}+\frac{\partial}{\partial \xi^k}\left(\mu J\xi_j^k\left(\xi_j^l\frac{\partial \overline{u_i}}{\partial \xi^l}+\xi_i^l\frac{\partial \overline{u_j}}{\partial \xi^l}\right)\right)-\frac{\partial}{\partial \xi^k}\left(\sigma_i^k\right) \tag{7}$$

where σ_i^k is the subgrid stress, which represents the contribution of smaller eddies. Mathematically this term has come from the non linear convective term of the momentum equation.

$$\sigma_i^k=J\overline{\rho}\left(\overline{U^k u_i}-\overline{U^k}\,\overline{u_i}\right)=J\overline{\rho}\overline{\xi_j^k}\left(\overline{u_i u_j}-\overline{u}_i\overline{u}_j\right) \tag{8}$$

Modeling of the sub grid stress

The SGS modeling in LES is similar to turbulence modeling in RANS. In RANS all effects of turbulence are modeled. As this includes the geometrically dependent large eddies, the modeling is to large extent problem dependent. But in case of LES, the SGS represents the role of smaller eddies which are more universal in behavior and less problem-dependent [25]. The SGS models describe the physics of smaller dissipative scales, which are computed from the resolved field. The SGS model should follow some physical and numerical constraints. As a physical constraints, the SGS model should conserve the basic properties, such as Galilean invariance and flow variables. And as a numerical constraints, a model should be less computationally expensive and it should not destabilized the code [35]. The most widely used Smagorinsky model [38] is based on the eddy viscosity Boussinesq's approach, which assume that the subgrid stresses are proportional to the mean filtered velocity gradients [14].

$$\sigma_i^k=J\overline{\xi_j^k}\left(-\mu_t\left(\xi_j^l\frac{\partial \overline{u_i}}{\partial \xi^l}+\xi_i^l\frac{\partial \overline{u_j}}{\partial \xi^l}\right)+\frac{2}{3}\delta_{ij}\overline{k}\right) \tag{9}$$

The momentum equation with Boussinesq's approximation

$$\frac{\partial J\overline{\rho}\,\overline{u_i}}{\partial t}+\frac{\partial \overline{\rho} J\overline{U^k}\overline{u_i}}{\partial \xi^k}=-\frac{\partial J\xi_i^k\left(\overline{p}+\frac{2}{3}\overline{k}\right)}{\partial \xi^k}+\frac{\partial}{\partial \xi^k}\left(\left(\mu+\mu_t\right)J\xi_j^k\left(\xi_j^l\frac{\partial \overline{u_i}}{\partial \xi^l}+\xi_i^l\frac{\partial \overline{u_j}}{\partial \xi^l}\right)\right) \tag{10}$$

With rearrangement of terms and introducing the $\mu_{eff}=(\mu+\mu_t)$.

$$\frac{\partial J\overline{\rho}\,\overline{u_i}}{\partial t}+\frac{\partial}{\partial \xi^k}\left(\overline{\rho}J\overline{U^k}\overline{u_i}-\mu_{eff}G^{kl}\frac{\partial \overline{u_i}}{\partial \xi^l}\right)=-\frac{\partial J\xi_i^k\left(\overline{p}+\frac{2}{3}\overline{k}\right)}{\partial \xi^k}+\frac{\partial}{\partial \xi^k}\left(\mu_{eff}J\xi_j^k\xi_i^l\frac{\partial \overline{u_j}}{\partial \xi^l}\right) \tag{11}$$

where the geometric diffusion coefficient G^{kl} is defined as

$$G^{kl}=\frac{A_j^kA_j^l}{J} \tag{12}$$

where A_j^k are the Cartesian area projections. For orthogonal coordinate system $G^{kl}=0$ for $k\neq l$.

The Smagorinsky Model

In the Smagorinsky model eddy viscosity is obtained by assuming that the energy transfer from the resolved scales to the small subgrid scales and the energy dissipation by the smaller subgrid scales are in equilibrium [38, 33]

$$\nu_t=\left(C_s\Delta\right)^2\left|\overline{S}\right| \tag{13}$$

$$|\overline{S}| = \sqrt{2\overline{S}_{ij}\overline{S}_{ij}} \tag{14}$$

$$\overline{S}_{ij} = \left(\xi_j^l \frac{\partial \overline{u_i}}{\partial \xi^l} + \xi_i^l \frac{\partial \overline{u_j}}{\partial \xi^l}\right) \tag{15}$$

in which $|\overline{S}|$ is a inner product of large-scale strain rate tensor, C_s is the Smagorinsky constant and Δ is the filter width. The Smagorinsky constant C_s is computed either from turbulence statistical theories or from DNS data base. The filter width Δ is computed by a model proposed by Deardorff [5]. The $C_s = 0.1$ was used in present LES simulation, while the filter width was obtained from.

$$\Delta = \left(J\delta\xi^l \delta\xi^2 \delta\xi^3\right)^{1/3} \tag{16}$$

The Dynamic Procedure

Some of the drawbacks with the Smagorinsky model are, inability to characterize the transitional flows i.e. laminar flow or flows near to walls, too dissipative in wall bounded flows, etc [44]. That is due to the fixed Smagorinsky constant C_s. The Smagorinsky constant C_s has to be tuned to characterize the transitional flows. This is accomplished either by an ad hoc correction such as Van Driest damping[41] or by the dynamic procedure proposed by Germano et al [10]. In the dynamic procedure the Smagorinsky constant is computed as a part of solution as a function of space and time. The dynamic procedure uses a test filter with width larger than the original filter, usually double the original filter size. The second test filter gives, when applied to the filtered momentum equation, a filtered subgrid scale stress tensor T_{ij} similar to the original SGS σ_{ij} [25]. The Smagorinsky constant in the dynamic procedure reads

$$C_s = \frac{1}{2}\frac{L_{ij}M_{ij}}{M_{kl}M_{kl}} \tag{17}$$

where tensor $M_{kl} = \overline{\Delta}^2 \widehat{|\overline{S}|\overline{S}_{kl}} - \widehat{\overline{\Delta}^2}\widehat{|\overline{S}|}\widehat{\overline{S}}_{kl}$ and $L_{ij} = \widehat{\overline{u}_i\overline{u}_j} - \widehat{\overline{u}}_i\widehat{\overline{u}}_j$
As it is mentioned that the constant C_s varies instantaneously with space and time and produces too much positive and too high negative value. Although negative values of the dynamic constant represent backward energy cascade mechanism, but a too negative constant C_s destabilizes the simulation [25, 35]. Many options have been studied to avoid this problem for instance averaging of constant C_s in homogeneous direction, clipping the constant C_s, and averaging the numerator and denominator of Eq. (17) in homogeneous direction [44]. In the present simulation averaging of the numerator and denominator along with clipping was used

$$< C_s >= \frac{1}{2}\frac{< L_{ij}M_{ij} >}{< M_{kl}M_{kl} >} \tag{18}$$

In Spider-LES the Smagorinsky constant is computed as $C_s = \max(< C_s >, 0)$, where the symbol $< . >$represents the spatial averaging.

The Structural Function Model

The Structural Function (SF) model or two point closure model is given by Métais and Lesieur[30, 23]. The eddy viscosity in the SF model is expressed as

$$\nu_t = 0.105 C_k^{-3/2} \Delta \sqrt{F_2(\mathbf{x}, t)} \tag{19}$$

where $F_2(\mathbf{x}, t)$ represents the second order velocity structure function and C_k is Kolmogorov constant. $F_2(\mathbf{x}, t)$ is built either with a six-point or four-point formulation inside the domain.

The four-point formulation is used near to the boundaries and six point formulation inside the domain. The six point formulation reads:

$$F_2(\mathbf{x},t) = \frac{1}{6}\sum_{i=1}^{3}\left(\left[\mathbf{u}(\mathbf{x},t) - \mathbf{u}(\mathbf{x}-\Delta x_i\mathbf{e}_i,t)\right]^2 + \left[\mathbf{u}(\mathbf{x},t) - \mathbf{u}(\mathbf{x}+\Delta x_i\mathbf{e}_i,t)\right]^2\right)\left(\frac{\Delta}{\Delta x_i}\right)^{2/3} \tag{20}$$

where $\mathbf{e}_i$ is the unit vector in x_i direction. The summation rule does not apply to the indices i.

General purpose code Spider-LES

The Spider code is an advanced computer program for the numerical simulation of steady, three-dimensional reacting and non-reacting flows. The code is based on the finite volume concepts and uses a non-staggered grid. The k-ε and Reynolds Stress equation models are used for turbulence modeling in Spider-3D. The Spider code uses power law scheme and second order up-winding scheme for convective fluxes. As pointed out by Piomelli [33] to resolve high wave-number turbulent fluctuations(SGS) accurately, either low-order schemes on very fine meshes, or higher-order schemes on coarser meshes are required. Although high-order schemes are very computationally demanding but their accuracy even with coarser meshes justify their use. A preliminary test, flow over square cylinder, showed that the default schemes in Spider3D were not suitable for LES. The LES approach was implemented in Spider code by employing the implicit box filter as mentioned above. In the Spider-LES the filtered NS Eq. (6) and Eq. (11). along with the SGS model are solved using finite volume technique.
In a non-staggered grid all the variables (pressure, velocities components and scalars) are stored at the cell center. For calculating convective fluxes, flow variables at cell faces are required. This is achieved by a discretization technique. Three discretization techniques, that is, the second order central scheme (CDS-2), the Quadratic Upwind Differencing Scheme (QUICK) and the fourth order central scheme (CDS-4) for convective fluxes are used in Spider-LES. The descriptions of these schemes are given in [9]. The viscous fluxes are approximated by central differences scheme of second-order accuracy. In Spider-LES non-staggered grid is used, which can produce unphysical oscillations i.e. checker-board pressure. Rhie and Chow [34] proposed an approach to avoid the unphysical oscillations. In this approach the convecting fluxes are calculated at the cell face with a special interpolation technique called momentum interpolation (MI). In the MI scheme velocities are computed from the discretized momentum equation at the face as well at the corresponding nodes. In addition to that cell face velocities are interpolated from the nodal values. Finally the cell face fluxes (mass fluxes) are formulated as a function of nodal velocities and pressure gradient.

Numerical Algorithm

In incompressible flow, density is not linked with pressure and for pressure-velocity coupling projection method [4] is used here. A three step (predictor-corrector-corrector) procedure is used here to solve the filtered continuity and momentum equations. In the predictor step the momentum equations are solved to obtain intermediate velocities field with old pressure values. This intermediate velocities field do not satisfy the continuity equation. In the first corrector step the pressure correction $p^{'}$ is calculated by solving the pressure correction $p^{'}$ Poisson equation [9] Eq. (21) with the intermediate filtered velocities $\overline{u}_i^*$ field from predictor step. The pressure correction Poisson equation [9] Eq. (21) is solved with strongly implicit procedure (SIP) of Stone [40].

$$\frac{\partial}{\partial x_i}\left(\frac{\partial p^{'}}{\partial x_i}\right) = \frac{1}{\triangle t}\left(\frac{\partial \rho \overline{u}_i^*}{\partial x_i}\right) \tag{21}$$

Here $\triangle t$ is the time step. In the second corrector step, velocities and old pressure are corrected with computed pressure correction field from first corrector step. The three-steps procedure is repeated until convergence. In Spider-LES, momentum equations are integrated with an explicit five stage fourth-order Runge-Kutta method by Carpenter et al. [3].

Problem Description

Large eddy simulations of a turbulent flow over backward facing step were performed with the Spider-LES. BFS shown in Fig. 1 was chosen for its apparent geometrical simplicity, but it involves relatively complex flow phenomena. This geometry is well suited to study the turbulence behavior under separation, recirculation and reattachment phenomena [31], which is of highly importance for many practical and engineering applications. The case was selected due to its similarity with bluff body combustion. Fuel and oxidizer can mix behind the bluff body. Alternatively, the reactants are pre-mixed and the flame is anchored at the bluff body. Furthermore a well established amount of numerical and experimental literature is available [21, 15, 17, 36, 20] for this case.

Computational Domain

Figure 1 shows the computational domain used for current simulation. In Fig. 1, x, y & z respectively, represent the longitudinal, vertical and spanwise directions. The longitudinal length L_x downstream of the step was $20h$ and channel length L_i, ahead of the step was $2.5h$. The dimensions in the vertical L_y and spanwise L_z directions were $6h$ and $4h$ respectively. The expansion ratio, the ratio of domain height downstream and upstream of the step was 1.2. The Reynolds number($Re_h = \rho U_0 h/\mu$) based on the step height h and free stream velocity U_0 was 5100. The domain dimensions and Reynolds number were same as the DNS of Le et al. [21]. The boundary layer thickness at the inlet $\delta_{99} = 1.2h$.

Simulation parameters

Two computational grids $(N_x \times N_y \times N_z)$= $(148 \times 62 \times 20)$ and $(148 \times 72 \times 20)$ were used with non-uniform distribution in the vertical and longitudinal directions and uniform grid distribution in the spanwise direction. The grid was refined close to the walls and in recirculation region. The time step in the current simulation was fixed at $\Delta_t = 0.05h/U_0$. The total simulation time was $500h/U_0$.

Boundary condition

Lower and Upper boundaries
A no-stress wall $v = 0, \frac{\partial u}{\partial y} = 0, \frac{\partial w}{\partial z} = 0$ consistent with DNS by Le et al. [21] was applied at the upper boundary. No-slip boundary conditions was used at all walls. The u, v and w are velocity components in longitudinal, vertical and spanwise direction respectively.
Spanwise boundaries
A no-stress wall $w = 0, \frac{\partial u}{\partial x} = 0, \frac{\partial v}{\partial y} = 0$ was used on the spanwise boundaries due to limited spanwise extent. Whereas cyclic boundary condition was used in DNS Le et al. [21].
Inlet boundaries
A mean turbulent profile by Spalart [39] at Re_θ = 670 supreimposed with a white noise was applied at inlet, where θ is the momentum thickness. The mean v and w were set equal to zero . At every time step, mean input velocity profile for a region y $\leq$ 1.2h was perturbed with random fluctuations.
Outflow boundaries
At outlet, where flow was completely developed the velocities gradient $\frac{\partial u_i}{\partial x_i} = 0$ were set equal

to zero.

Results and discussion

LES simulations over BFS was carried out for the five cases as shown in Table-1. Run-1 and Run-2 were carried out to examine the influence of grid. Run-3 and Run-4 were for understanding the influence of the SGS model and Run-5 was for understanding the effect of discretization schemes. Different flow parameters, reattachment length, skin friction coefficient, mean longitudinal, vertical velocity profiles and turbulent intensity were computed and compared with DNS data set Le et al. [21]. These parameters were averaged in time and along the spanwise direction. The mean longitudinal, vertical velocity profiles and turbulent intensity were non dimensionalized with inflow free stream velocity U_0

Table 1: LES test cases for flow over BFS

Runs	Scheme	SGS model	Grid	Remarks
Run-1	QUICK	Structure function(SF)	$(148 \times 62 \times 20)$	Influence of grid
Run-2	QUICK	Structure function(SF)	$(148 \times 72 \times 20)$	Influence of grid
Run-3	QUICK	Dynamic (DM)	$(148 \times 72 \times 20)$	Influence of SGS model
Run-4	QUICK	Smagorinsky	$(148 \times 72 \times 20)$	Influence of SGS model
Run-5	CDS-4	Smagorinsky	$(148 \times 72 \times 20)$	Influence of discretization

The Skin Friction Coefficient

The skin friction coefficient C_f is computed as:

$$C_f = \frac{\tau_w}{1/2\rho U_0^2} \tag{22}$$

where $\tau_w = \rho\left(\nu\frac{\partial u}{\partial y}\right)_{wall}$ is the wall shear stress. Fig 2 shows the mean skin friction coefficient C_f obtained with the Spider-LES compared to that obtained from the DNS of Le et al. [21] along the longitudinal direction. The negative peak of skin friction coefficient C_f was underpredicted for the all runs. The reason for the underprediction was poor grid resolution near to the wall. This was confirmed by running one more simulation with fine grid and it was observed from Run-1 and Run-2 that the C_f improved with grid resolution. It was also observed from the Run-2, Run-3 and Run-4 that the C_f prediction with the SF model was slightly better than the other models, that was because the SF model is 20% less diffusive than the Smagorinsky model [23]. The effect of the discretization scheme could be observed from the Run-4 and Run-5 in Fig. 2, which showed that the CDS-4 predicted better reattachment length $7.0h$ than the QUICK scheme $7.2h$. There were some oscillations in C_f for the Run-4 in recovery zone due to low grid resolution caused by grid stretching. The negative C_f peak was shifted downstream for the most of the runs. A shift in the peak was attributed to the long recirculation zone as shown in Fig 3. Fig 3 shows the mean stream function, where primary and secondary recirculation zones were well captured.

Reattachment length

The mean reattachment location X_r was computed by the three method as proposed by Le et al. [21]. (a) The longitudinal distance where $\tau_w = 0$, as shown in Fig. 2. (b) The location at which

the mean dividing streamline (ψ = 0) touched the wall, as shown in Fig 3. (c) The longitudinal distance at which mean longitudinal velocity $u = 0$ at the first grid point normal to the wall, as shown in Figure 4 & 6. The reattachment length was X_r= $7.2h$ to $7.4h$ with different SGS model. The computed reattachment length X_r was far from the DNS value $(X_r = 6.28h)$ of Le et al. [21] and the experimental value $(X_r = (6.0 \pm 0.15)h)$ of Jovic and Driver [17]. This was due to fact that the inflow boundary condition used in the current simulation was not consistent with inflow boundary condition used by DNS Le et al. [21]. Increase of the reattachment length and delay in the transition of the shear layer was caused due to the absence of the turbulent longitudinal vortices's associated with the inflow boundary layer [23]. It was also observed that the recirculation length did not change much with SGS model, because all models were eddy viscosity based.

A LES of BFS carried out by Dubief and Delcayre [6] observed a recirculation length of $7.2h$ at the same Reynolds number of 5100. The inflow boundary condition was mean velocity profile [39] perturbed with white noise and the SGS model was the filtered structural function (FSF) with the four-point formulation. A LES of BFS carried out by Aider and Danet [1] observed a recirculation length of 5.8h when the mean velocity profile [39] perturbed with white noise was used at inflow. However, in more realistic case, inflow boundary with precursor simulation(PS) they observed a reattachment length of $5.2h$. The SGS model used in their simulation was the filtered structural functional (FSF) with the four-point formulation. They observed the shorter reattachment length even though outflow boundary condition was used at upper boundary, which is equivalent to an infinite expansion ratio. According to kuehn [20] the reattachment length increases with an increase in expansion ratio. Simons et al. [37] also carried out LES over BFS and they observed the recirculation length of 6.6h with Smagorinsky SGS models. The authors concluded that the numerical accuracy of the solver and grid refinement have a stronger influence on the BFS simulation than the details of the SGS model. The present results also support this finding

Mean Longitudinal and Vertical Velocities

As it was observed that the reattachment length was overpredicated for all the cases. Westphal and Johnston [43] concluded that the averaged flow parameters (C_f, u_i, etc) were independent of the initial conditions, geometrical parameters and boundary conditions with respect to the normalized coordinate $X^* = \frac{x - X_r}{X_r}$. This was also confirmed by Dubief and Delcayre [6] and Aider and Danet [1]. In the present study the normalized coordinates X^* were used for comparison of our LES results with the DNS of Le et al. [21]. Figure 4 shows the comparison between computed LES (Run-2, Run-3 and Run-4) and the DNS data by Le et al. [21] for the non dimensional mean vertical velocity profiles. The comparison was made at four locations in the recirculation (X^* = -0.333), reattachment (X^* = 0) and recovery regions (X^* = 0.66, and X^* = 1.497), where the DNS data were available [21]. The computed results compared well with the DNS results at the reattachment (X^* = 0) and the recovery region (X^* = 0.66). The longitudinal velocity was under predicated at (X^* =-0.333) especially for $y \leq 0.5h$, that caused underprediction in skin friction coefficient C_f. It was also observed that the longitudinal velocity was overpredicated at (X^* = 1.497). This was because the outflow boundary condition used was a zero velocity gradient $\frac{\partial u_i}{\partial x_i} = 0$ whereas in the DNS a convective boundary condition $\frac{\partial u_i}{\partial t} + c\frac{\partial u_i}{\partial x_i} = 0$ was used. In addition, a too coarse grid at this location produced too much diffusion. Figure 6 shows a comparison between the computed LES (Run-4 and Run-5) and the DNS data for the mean streamwise velocity profiles. The comparison was made at the same four locations and the computed results compared well with the DNS data at all locations

including at (X^* = 1.497). This was because even though grid used in this region was coarse but the CDS-4 is less diffusive in nature compared to the QUICK scheme. It was also observed that the longitudinal velocity profiles matched well with the DNS for $y \geq 2h$, that was because upper boundary condition (no stress wall) was consistent with the DNS simulation. Figure 5 shows vertical velocity profile of the present LES, the DNS and the experiments [17]. The computed LES results compared satisfactory with DNS for $y \geq 2h$ due to same upper boundary condition. Discrepancy between the vertical velocity profile of the DNS by Le et al [21] and the experiments of Jovic and Driver [17] was observed, especially for the region $y \geq 1h$ due to difference in upper boundary condition. Eaton and Johnston [7] reviewed the subsonic flow over BFS. They compared the mean velocity profile at normalized coordinate $X^* = 0$ and they observed the differences in the results for the region $y \geq 1h$ due to the different upper boundary condition. Aider and Danet [1] overpredicted the mean longitudinal and vertical velocity for $y \geq 1h$ due to different upper $(\partial u_i/\partial y = 0)$ boundary condition.

Turbulence intensity and Reynolds shear stress

Figure 7 shows time-averaged (a) longitudinal $\langle u^{'}u^{'}\rangle^{1/2}/U_0$, (b) vertical $\langle v^{'}v^{'}\rangle^{1/2}/U_0$, (c) spanwise $\langle w^{'}w^{'}\rangle^{1/2}/U_0$ turbulent intensities and (d) Reynolds shear stress component $\langle u^{'}v^{'}\rangle/U_0^2$ computed with current LES (Run-2,Run-3 and Run-4) compared to the DNS of Le et al. [21]. Where $u^{'}$, $v^{'}$ and $w^{'}$ are the velocity fluctuation in longitudinal, vertical and spanwise direction. The comparison was made at the same four location. The longitudinal turbulence intensity predicted well with DNS especially for the region $y \leq 1.0h$ and it was underpredicted for the region $2.2h \geq y \geq 1.0h$ at the reattachment (X^* = 0) and the recirculation (X^* = -0.333). This could be due to two reasons: the first reason was the poor grid resolution for the region $1.0h \leq y \leq 6.0h$, which has reduced the turbulent intensity due to inherent numerical diffusion of QUICK scheme. On the other hand the CDS-4 scheme is less diffusive in nature and predicted more turbulence intensity than the QUICK scheme as shown in Figure 8. The another reasons was that the inflow boundary condition was not computed as deterministically as it was done in the DNS. The longitudinal turbulent intensity $\langle u^{'}u^{'}\rangle^{1/2}/U_0$ was slightly overpredicted at recovery region (X^* = 0.66, and X^* = 1.497). The vertical turbulent intensity $\langle v^{'}v^{'}\rangle^{1/2}/U_0$ was underpredicted at recirculation(X^* = -0.333) and the prediction is better at the reattachment (X^* = 0). Figures 7 & 8 show the better agreement of Reynolds shear-stress component $\langle u^{'}v^{'}\rangle/U_0^2$ for the region $y \leq 1.0h$.

Conclusions

Large Eddy simulation approach was implemented in the Spider-3D code. Higher order QUICK and CDS-4 disscretization schemes for convective terms were implemented. Three Subgrid Stress (SGS) Models i.e. Smagorinsky, dynamic and structural function model were studied and implemented in the Spider-LES. The LES was carried out for a flow over the backward-facing step at moderate Re = 5100. Total five simulation were carried out to understand the influences of grid, the discretization scheme and the SGS models. The LES studies showed overall satisfactory agreement with the existing DNS data Le et al. [21] for a relatively coarser mesh about 40 times lesser than the DNS. The negative peak of skin friction coefficient was underpredicted due to poor grid resolution near to the wall. The mean reattachment length was overpredicated due to inconsistent inflow boundary condition. The reattachment length in the longitudinal direction was $7.2h - 7.4h$ with different SGS model. Effect of the sub grid modelling was minimal, that is because all studied models were eddy viscosity based. The reattachment length prediction was better with the CDS-4 than the QUICK scheme. The mean longitudinal velocity profile, vertical

velocity profile and the Reynolds stresses compared satisfactory with DNS data set Le et al. [21] with respect to normalized coordinated $X^* = \frac{x - X_r}{X_r}$. The discrepancies in results between the DNS and the present LES were due to the fact that the length of both primary and secondary recirculation zone were overpredicted in the present LES.

References

[1] J. L.Aider and A.Danet Large-eddy simulation study of upstream boundary conditions influence upon a backward-facing step flow *Comptes Rendus Mècanique*, **vol.334**(7), 447 – 453, 2006.

[2] L. C.Berselli, T.Iliescu and W. J.Layton *Mathematics of Large Eddy Simulation of Turbulent Flows* Springer Verlag, 2006.

[3] M. H.Carpenter and C. A.Kennedy. Fourth-order 2N-storage runge-kutta schemes NASA Technical Memorandum NASA -TM 109112, pages 1-26, June 1994.

[4] A. J.Chorin and J. E.Marsden *A Mathematical Introduction to Fluid Mechanics* 3rd ed. Springer Verlag, 1993.

[5] J. W.Deardorff A numerical study of three-dimensional turbulent channel flow at large Reynolds numbers *Journal of Fluid Mechanics*, **vol.41**, 453–480, 1970.

[6] Y.Dubief and F.Delcayre On coherent-vortex identification in turbulence *Journal of Turbulence*, **vol.1**, 1–22, Dec. 2000.

[7] J. K.Eaton and J. P.Johnston A review of research on subsonic turbulent flow reattachment *AIAA Journal*, **vol.19**, 1093–1100, Sept. 1981.

[8] I. S.Ertesvåg *Turbulent flow and combustion (In Norwegian)* Tapir Academic Publisher, Trondheim, 2000.

[9] J. H.Ferziger and M.Peric *Computational Methods for Fluid Dynamics* Springer Verlag, 2001.

[10] M.Germano, U.Piomelli, P.Moin and W. H.Cabot A dynamic subgrid-scale eddy viscosity model *Physics of Fluids A: Fluid Dynamics*, **vol.3**(7), 1760–1765, 1991.

[11] I. R.Gran and B. F.Magnussen A numerical study of a bluff-body stabilized diffusion flame. part 1. influence of turbulence modeling and boundary conditions *Comb.Sci.Tech.*, **vol.119**, 171–190, 1996.

[12] I. R.Gran and B. F.Magnussen A numerical study of a bluff-body stabilized diffusion flame. part 2. influence of combustion modeling and finite-rate chemistry *Comb.Sci.Tech.*, **vol.119**, 191–217, 1996.

[13] A.Gruber *Direct numerical simulation of turbulent combustion near solid surfaces.* Dr. ing thesis **N**o. 2006:14, Norwegian University of Science and Technology, Trondheim, 2006.

[14] J. O.Hinze *Turbulence* McGraw-Hill Publishing Co., New York, 1975.

[15] K.Isomoto and S.Honami The effect of inlet turbulence intensity on the reattachment process over a backward-facing step *ASME Transactions Journal of Fluids Engineering*, **vol.111**, 87–92, Mar. 1989.

[16] S. A.Jordan A Large-Eddy Simulation Methodology in Generalized Curvilinear Coordinates *Journal of Computational Physics*, **vol.148**, 322–340, Jan. 1999.

[17] S.Jovic and D. M.Driver Backward-facing step measurements at low Reynolds number, Re=5000 *NASA Technical Memorandum NO:108807*, pages 1–24, Feb. 1994.

[18] W. W.Kim and S.Menon An unsteady incompressible Navier-Stokes solver for large eddy simulation of turbulent flows *International Journal for Numerical Methods in Fluids*, **vol.31**, 983–1017, Nov. 1999.

[19] T.Kobayashi Large eddy simulation for engineering applications *Fluid Dynamics Research*, **vol.38**(2-3), 84–107, 2006.

[20] D. M.Kuehn Effects of Adverse Pressure Gradient on the Incompressible Reattaching Flow over a Rearward-Facing Step *AIAA Journal*, **vol.18**, 343–344, Mar. 1980.

[21] H.Le, P.Moin and J.Kim Direct numerical simulation of turbulent flow over a backward-facing step *Journal of Fluid Mechanics*, **vol.330**, 349–374, Jan. 1997.

[22] S. K.Lele Compact Finite Difference Schemes with Spectral-like Resolution *Journal of Computational Physics*, **vol.103**, 16–26, Nov. 1992.

[23] M.Lesieur, O.Mètais and P.Comte *Large-Eddy Simulations of Turbulence* Cambridge University Press, 2005.

[24] D.Lilly On the application of the eddy viscosity concept in the inertial subrange of turbulence Technical report, NCAR Manuscript, 1966.

[25] B.M. Large eddy simulation of the subcritical flow past a circular cylinder: numerical and modeling aspects *International Journal for Numerical Methods in Fluids*, **vol.28**(9), 51281–1302, 1998.

[26] M. C.Melaaen *Analysis of curvilinear non-orthogonal coordinates for numerical calculation of fluid flow in complex geometries.* Dr. ing thesis **N**o. **NTH** 1991:15, University in Trondheim(NTH), 1990.

[27] M. C.Melaaen Calculation of fluid flows with staggered and nonstaggered curvilinear nonorthogonal grids-A comparison *Numerical Heat Transfer part B*, **vol.21**, 21–39, Feb. 1992.

[28] M. C.Melaaen Calculation of fluid flows with staggered and nonstaggered curvilinear nonorthogonal grids-The theory *Numerical Heat Transfer part B*, **vol.21**, 1–19, Feb. 1992.

[29] A.Meri and H.Wengle *DNS and LES of turbulent backward-facing step flow using 2ND-and 4TH-order discretization*, pages 99–114 Advances in LES of Complex Flows,Springer Netherlands, 2002.

[30] O.Mètais and M.Lesieur Spectral large-eddy simulation of isotropic and stably stratified turbulence *Journal of Fluid Mechanics*, **vol.239**, 157–194, June 1992.

[31] M.Mizukami, N. J.Georgiadis and M. R.Cannon A comparative study of computational solutions to flow over a backward-facing step In *its The Fifth Annual Thermal and Fluids Analysis Workshop p 523-530 (SEE N94-23634 06-34)*, pages 523–530, Nov. 1993.

[32] A.Nakayama and S. N.Vengadesan On the influence of numerical schemes and subgrid-stress models on large eddy simulation of turbulent flow past a square cylinder *International Journal for Numerical Methods in Fluids*, **vol.38**, 227–253, Jan. 2002.

[33] U.Piomelli Large-eddy simulation: achievements and challenges *Progress in Aerospace Sciences*, **vol.35**(4), 335 – 362, 1999.

[34] C. M.Rhie and W. L.Chow Numerical study of the turbulent flow past an airfoil with trailing edge separation *AIAA Journal*, **vol.21**, 1525–1532, Nov. 1983.

[35] P.Sagaut *Large Eddy Simulation for Incompressible flows* Springer Verlag, 2006.

[36] A.Silveira Neto, D.Grand, O.Mètais and M.Lesieur A numerical investigation of the coherent vortices in turbulence behind a backward-facing step *Journal of Fluid Mechanics*, **vol.256**, 1–25, 1993.

[37] E.Simons, M.Manna and C.Benocci *Parallel multi-domain large-eddy simulation of the flow over a backward-facing step at Re=5100*, pages 115–130 Advances in LES of Complex Flows,Springer Netherlands, 2002.

[38] J.Smagorinsky General circulation experiments with the primitive equations *Monthly Weather Review*, **vol.91**, 99–110, 1963.

[39] P. R.Spalart Direct simulation of a turbulent boundary layer up to **Re** 1410 *Journal of Fluid Mechanics Digital Archive*, **vol.187**, 61–98, 1988.

[40] H. L.Stone Iterative solution of implicit approximations of multidimensional partial differential equations *SIAM Journal on Numerical Analysis*, **vol.5**(3), 530–558, 1968.

[41] E. R.Van Driest 1956 on turbulent flow near a wall *J . Aero. Sci*, **vol.23**, 1007–1011, 1956.

[42] M.Vinokur An analysis of finite-difference and finite-volume formulations of conservation laws *Journal of Computational Physics*, **vol.81**(1), 1 – 52, 1989.

[43] R. V.Westphal and J. P.Johnston Effect of initial conditions on turbulent reattachment downstream ofa backward-facing step *AIAA Journal*, **vol.22**, 1727–1732, Dec. 1984.

[44] Y.Zang, R. L.Street and J. R.Koseff A dynamic mixed subgrid-scale model and its application to turbulent recirculating flows *Physics of Fluids A: Fluid Dynamics*, **vol.5**(12), 3186–3196, 1993.

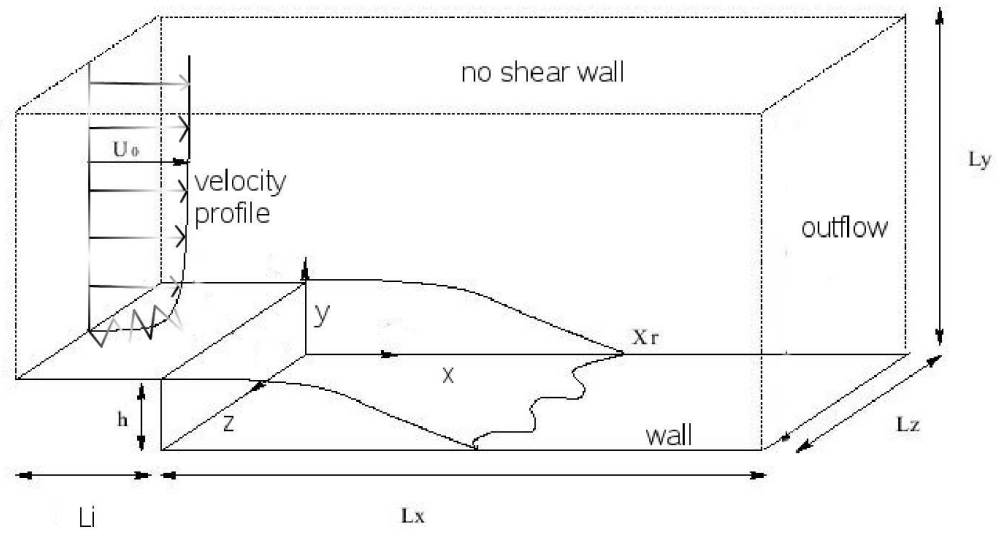

Figure 1: Backward Facing Step (BFS) configuration

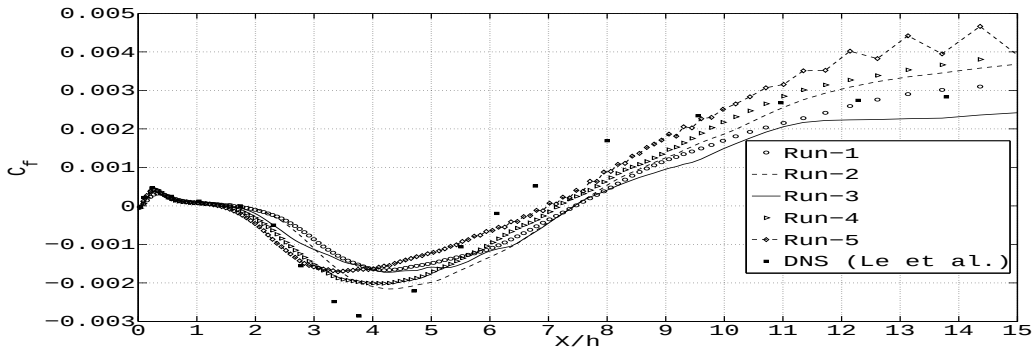

Figure 2: Mean skin friction coefficient along the longitudinal direction

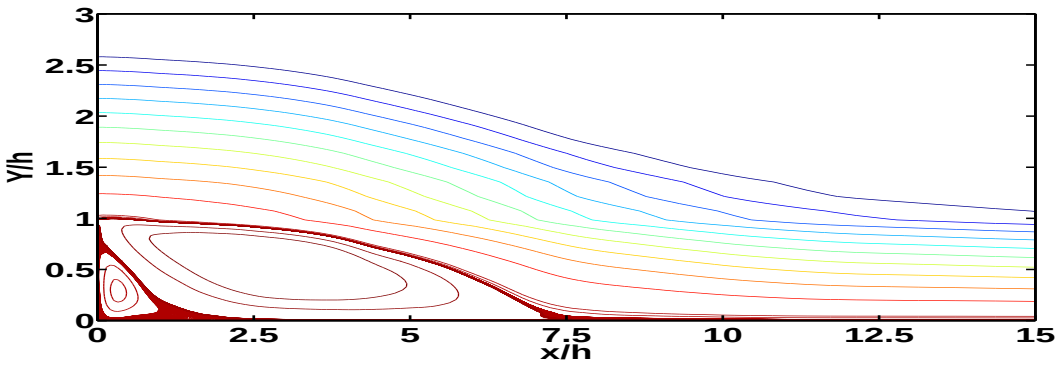

Figure 3: Stream function of mean flow averaged in space and time for Run-3

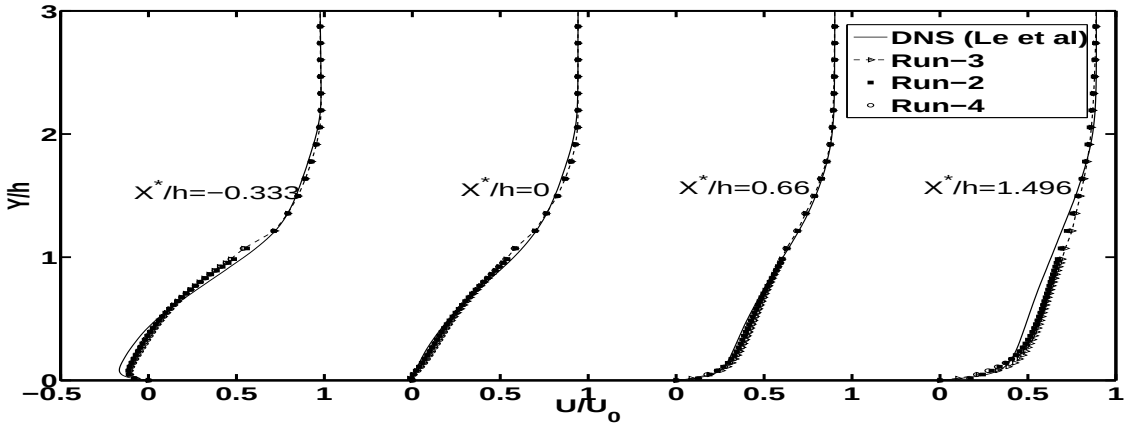

Figure 4: Mean longitudinal velocity profiles at four different streamwise positions downstream of the step, for Run-2, Run-3 and Run-4 compared to DNS results of Le et al. [21]

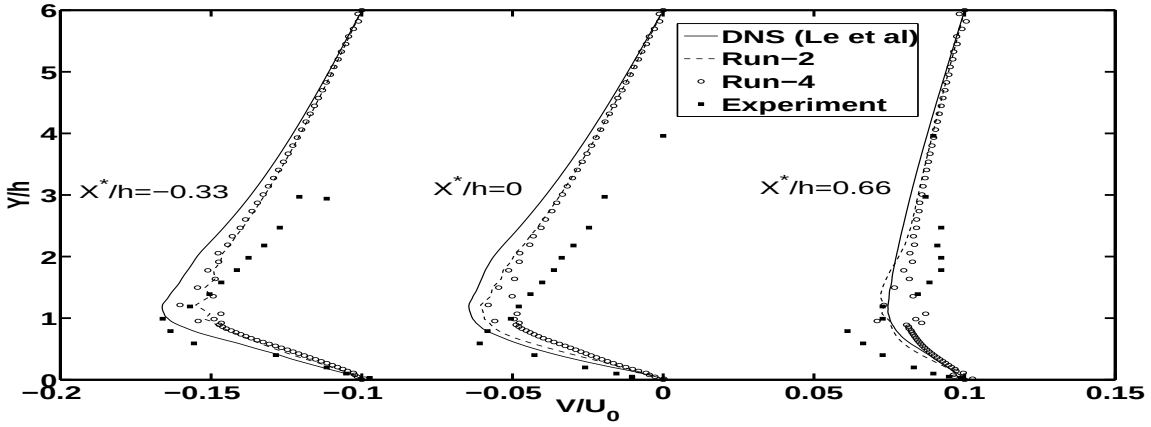

Figure 5: Mean vertical velocity profiles at four different streamwise positions downstream of the step, for Run-2 and Run-4 compared to DNS results of Le et al. [21] and experiment of Jovic and Driver [17]

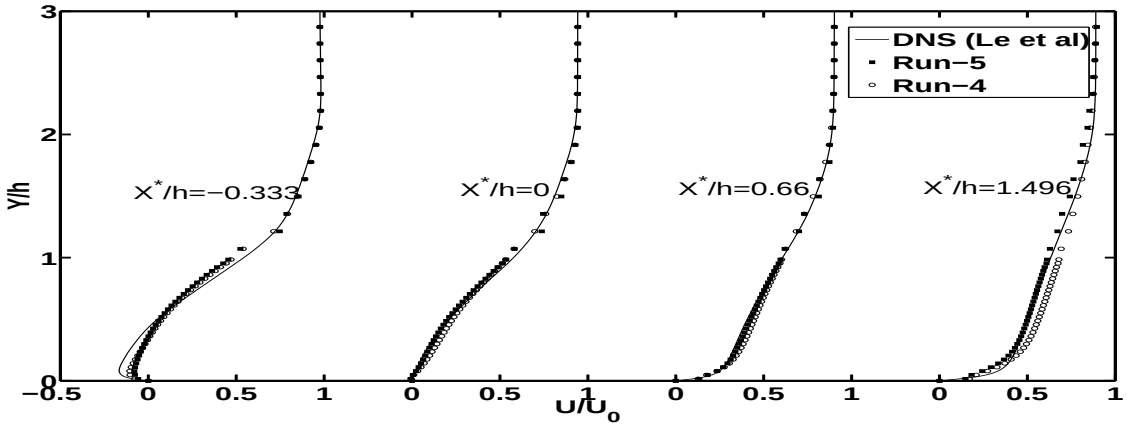

Figure 6: Mean longitudinal velocity profiles at four different streamwise positions downstream of the step, for Run-4 and Run-5 compared to DNS results of Le et al. [21]

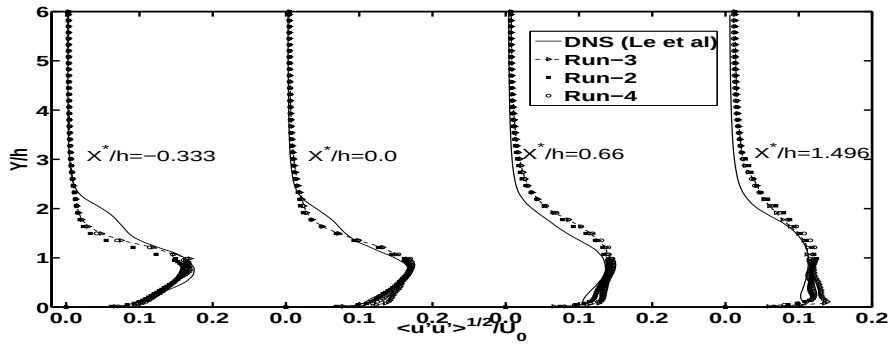

(a)

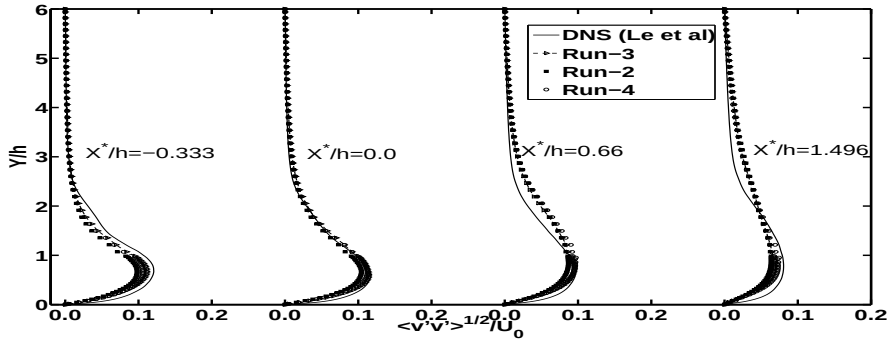

(b)

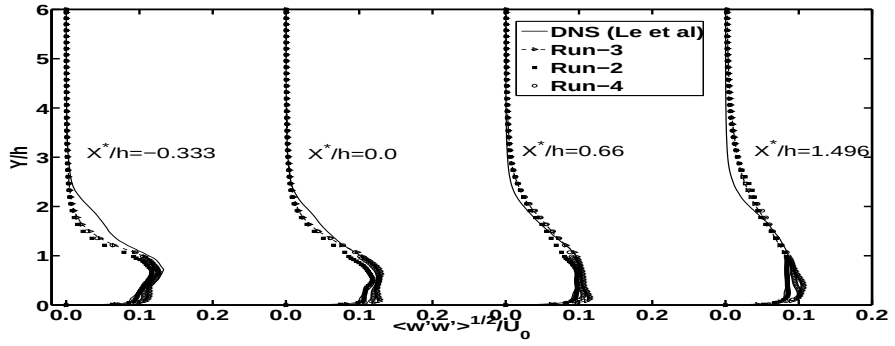

(c)

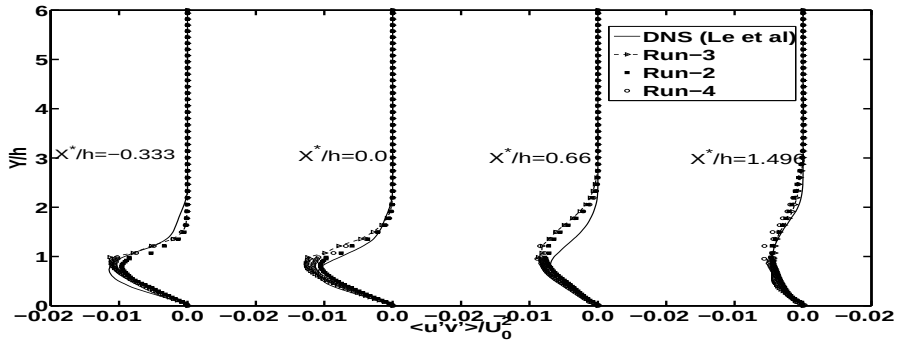

(d)

Figure 7: Square roots of non-dimensional mean Reynolds stresses. (a) $\langle u^{'}u^{'}\rangle^{1/2}/U_0$, (b) $\langle v^{'}v^{'}\rangle^{1/2}/U_0$, (c) $\langle w^{'}w^{'}\rangle^{1/2}/U_0$, (d) $\langle u^{'}v^{'}\rangle/U_0^2$ at four different streamwise positions downstream of the step for Run-2, Run-3 and Run-4 compared to DNS results of Le et al. [21]

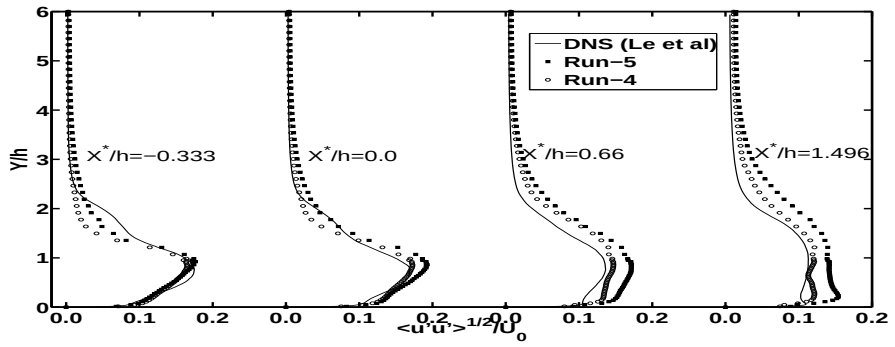

(a)

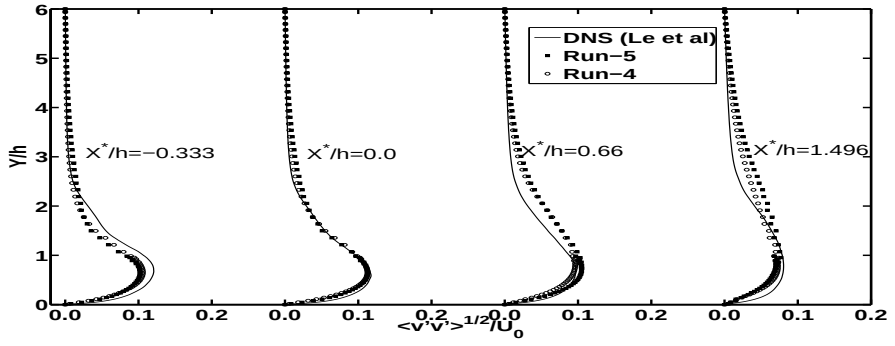

(b)

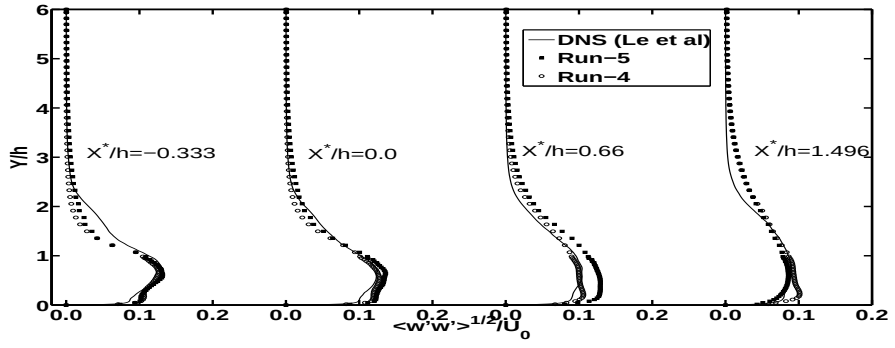

(c)

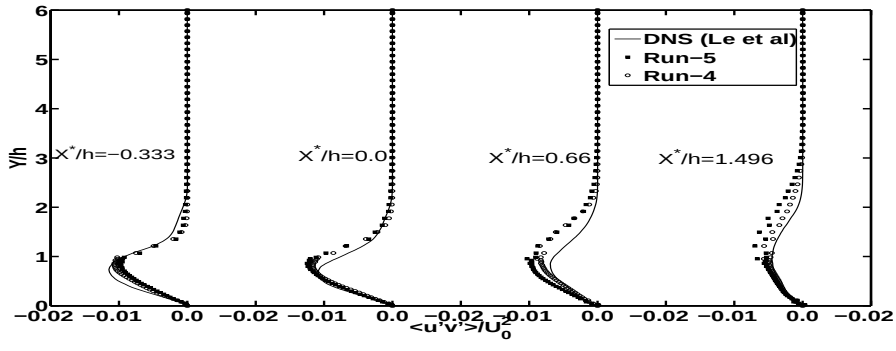

(d)

Figure 8: Square roots of non-dimensional mean Reynolds stresses. (a) $\langle u^{'}u^{'}\rangle^{1/2}/U_0$, (b) $\langle v^{'}v^{'}\rangle^{1/2}/U_0$, (c) $\langle w^{'}w^{'}\rangle^{1/2}/U_0$, (d) $\langle u^{'}v^{'}\rangle/U_0^2$) at four different streamwise positions downstream of the step for Run-4 and Run-5 compared to DNS results of Le et al. [21]